Journal of Power Sources 196 (2011) 1769–1775

Contents lists available at ScienceDirect

Journal of Power Sources

journal homepage: www.elsevier.com/locate/jpowsour

Quantifying the water content in the cathode of enzyme fuel cells via neutron imaging

D.S. Aaron[a], A.P. Borole[b], D.S. Hussey[c], D.L. Jacobson[c], S. Yiacoumi[a], C. Tsouris[a,b,*]

[a] School of Civil and Environmental Engineering, Georgia Institute of Technology, Atlanta, GA 30332, USA
[b] Oak Ridge National Laboratory, 1 Bethel Valley Road, Oak Ridge, TN 37831-6161, USA
[c] National Institutes of Standards and Technology, 100 Bureau Dr., Mail Stop 8461, Gaithersburg, MD 20899, USA

ARTICLE INFO

Article history:
Received 12 July 2010
Received in revised form
27 September 2010
Accepted 29 September 2010
Available online 8 October 2010

Keywords:
Enzyme fuel cell
Neutron imaging
Laccase
Three-dimensional cathode
Water management

ABSTRACT

Neutron imaging was used to study cathode water content over time in a three-dimensional-cathode enzyme fuel cell (EFC). A porous carbon felt cathode allowed air to flow through the electrode. A solution with laccase and a mediator formed an aqueous layer on the electrode surface. Water loss was observed *in situ* via neutron imaging for varying experimental conditions, including flow rates of hydrogen and air, cathode inlet humidity, volume of enzyme solution, and its composition. Cathode water loss occurred for all experimental conditions, but the loss rate was noticeably reduced when a high-salt-concentration enzyme solution was used in the cathode in conjunction with increased humidity in the air feed stream. Results from neutron imaging and power density analysis were used in analyzing the causes that could contribute to EFC water loss. An increase in temperature due to the exothermic cathode reaction is considered a plausible cause of cathode water loss via evaporation. This is the first reported application of neutron imaging as a technique to study EFC water management. The results suggest that neutron imaging can be employed to provide a better understanding of EFC phenomena and thereby contribute to design and operational improvements of EFCs.

1. Introduction

Enzyme fuel cells (EFCs) have emerged as a potentially promising alternative to the more expensive platinum-based polymer-electrolyte-membrane fuel cells (PEMFCs). EFCs employ biologically derived enzymes to catalyze the electrode reactions in a fuel cell, replacing precious-metal catalysts as part of an effort to reduce the cost of fuel cells. These fuel cells operate on similar principles and designs as traditional PEMFCs that run on hydrogen [1]. The enzyme laccase from the fungus *Trametes versicolor* has been utilized in a three-dimensional cathode design by Borole et al. [2] to catalyze the reduction of oxygen to water and provide a relatively high power density. The three-dimensional design facilitates oxygen transport to the laccase enzyme. As with PEMFCs, water management is a critical issue in EFC operation to ensure optimal power production and longevity. Water provides the medium for proton diffusion from the anode, through the polymer electrolyte membrane (PEM), and into the cathode [3]. For a mediated-electron-transfer EFC, water also provides a medium for shuttling electrons between the aqueous catalyst and the electrode [4]. Hudak et al. [5] observed that long-term EFC activity is unstable due, in part, to water loss in the cathode. Enzyme activity in a direct-electron transfer laccase cathode has been shown to be steady over hundreds of hours of operation, thus water management is of great interest for providing long-term power from an EFC [6]. One method to reduce water loss is to utilize a microfluidic EFC, but these devices are not considered promising for larger-scale power applications because they rely on very small designs [7,8]. Because a proper water balance is critical to macroscale EFC operation, a technique to measure the water loss rate in situ during EFC operation is very desirable.

Neutron imaging has been demonstrated as a useful technique for studying water evolution and distribution in PEMFCs without disturbing the fuel cell operation [9]. Because hydrogen has a larger total neutron scattering cross section than other fuel cell materials (e.g., carbon, oxygen, and aluminum), neutron imaging is a powerful technique for measuring *in situ* water content, as opposed to other techniques such as X-ray. Gaseous hydrogen makes little contribution to neutron attenuation because it is much less dense than water. Early experiments oriented the fuel cell plane normal to the neutron beam, resulting in a "face-on" view that allowed quantification of the in-plane water content; however, this approach cannot distinguish anode water from cathode water [9,10]. This orientation was primarily made necessary by the relatively low

* Corresponding author at: School of Civil and Environmental Engineering, Georgia Institute of Technology, Atlanta, GA 30332, USA. Oak Ridge National Laboratory, 1 Bethel Valley Road, Oak Ridge, TN 37831-6161, USA. Tel.: +1 865 241 3246.
E-mail address: tsourisc@ornl.gov (C. Tsouris).

0378-7753/$ – see front matter © 2010 Elsevier B.V. All rights reserved.
doi:10.1016/j.jpowsour.2010.09.095

resolution (i.e., 250 μm) of the available detectors. High-resolution neutron imaging (approximately 25-μm resolution) allowed the water content in the anode, PEM, and cathode of a PEMFC to be resolved separately and monitored over time during operation. This was achieved by orienting the fuel cell for an "edge-on" view with respect to the beam [11]. The water content in each region of the operating PEMFC can be studied in the context of operating conditions, including current density, to provide a better understanding of the link between local heating, current output, and water content [12].

As in many types of fuel cells, water management is important to the performance of EFCs. Neutron imaging has been recently employed to successfully monitor the water content in PEMFCs. This technique is investigated here for the first time for in situ measurements of water content and evolution in an operating EFC at varying operating conditions. Efforts are also made to reduce water loss rates, and the results are evaluated via neutron imaging.

2. Materials and methods

2.1. EFC design

Initial experiments were performed at Oak Ridge National Laboratory (ORNL) to study the power density behavior at a variety of operating conditions. A three-dimensional cathode EFC was constructed with materials that exhibited low neutron attenuation. Polytetrafluoroethylene (PTFE) plates (from Professional Plastics[1]) were cut to 5 cm × 5 cm to serve as endplates. The cathode compartment was made of PTFE as well, with a thickness of 0.430 cm and an open internal area of 0.18 cm × 0.13 cm. The anode compartment was 0.075-cm thick PTFE with the same open area as the cathode. This material was used due to its low neutron cross section, as well as ease of handling and shaping. Graphite electrodes were used as current collectors in both the anode and cathode; gold was not used due to its activation by neutron irradiation. The construction of this EFC was designed to facilitate neutron imaging, with less emphasis on optimized power production.

The anode was an electrode made of carbon cloth impregnated with platinum particles (Fuel Cell Store, Inc.) with an area of 1 cm^2. A loose-weave carbon cloth of the same area as the anode served as a gas diffusion layer and spacer for the anode. The cathode was carbon felt (Alfa Aesar) cut to 1 cm^2 with a thickness of 0.32 cm. The porosity for this carbon felt was 83% and was made hydrophilic via a 5-min plasma treatment (Harrick Plasma Company, PDC-32G). The PEM used was Nafion 115. The cathode solution was composed of enzyme, buffer, and mediator in water. The enzyme was laccase from *Trametes versicolor* with a specific activity of 21.7 units mg^{-1} (Sigma, St. Louis, Missouri). The buffer was citrate at pH 4, and the mediator was 2,2′-azinobis(3-ethylbenzothiazoline-6-sulfonate) (ABTS). Previous experiments by Borole et al. [2] established that an optimal volume of cathode solution for a similar-geometry EFC was 100 μL, with a 100:1 molar ratio of ABTS:laccase. Fig. 1 is a schematic of the EFC used in these experiments.

2.2. Neutron imaging and EFC control

Neutron imaging studies were conducted at the National Institute of Standards and Technology (NIST) Neutron Imaging Facility,

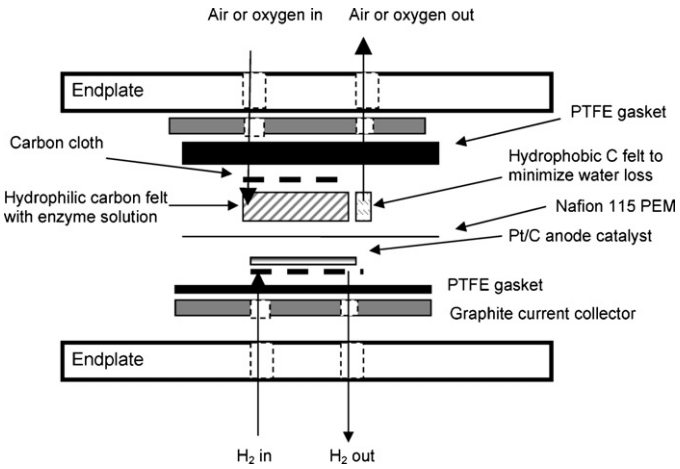

Fig. 1. Schematic of EFC used for imaging experiments. Only the enzyme solution was a strong neutron attenuator in this setup.

which includes a full suite of equipment for fuel cell operation, control, and analysis, and is integrated with the beam for neutron imaging [13]. A fuel cell test stand was employed to control all operational parameters, including feed flow, feed humidity, and feed composition. The load was controlled via a variable 2 kΩ resistor since the current developed by the 1-cm^2 EFC was too small for the test stand controller. Because the PTFE endplates of the EFC did not allow for good temperature control of the EFC, all experiments were performed at room temperature (approximately 24 °C). Supersaturated humidity conditions—that is, relative humidity (RH) greater than 100%—were achieved by raising the temperatures of the humidifying bottles above cell temperature. The lines between the humidifiers and EFC were also heated 5 °C above the humidifier bottle temperature to mitigate condensation in the feed lines. Power density measurements were performed after the EFC achieved steady-state output, roughly 1 h after enzyme solution injection and initiation of feed flows. The beam had a fluence rate of approximately 5.1×10^6 cm^{-1} s^{-1}. The detector used in this work was a micro-channel plate detector with a cross-delay line readout that had a 25 μm spatial resolution. Each image had an exposure time of 5 min.

2.3. Dry images

"Dry images" were taken prior to each experiment to provide the basis for water content measurement. Images of the EFC were taken after flowing dry nitrogen gas through the EFC and prior to injection of the cathode enzyme solution. The EFC was not removed from the test stand between experiments, so the same membrane was used for each experiment. This was expected to result in a dried-out EFC after a sufficient period of time, with no water present. By this reasoning, any change in neutron attenuation during operation, compared to the dry images, would be due to the presence of water. The water content was calculated by simply dividing the dry-image neutron intensity from the wet-image neutron intensity and assigning the difference to neutron attenuation by water via the Lambert–Beer law [14].

The fuel cell was placed edge-on in the beam, such that the image projected onto the detector was a side view of the EFC (see orientation in Fig. 1). Table 1 shows the operating conditions explored in this study. Fresh cathode enzyme solution was injected into the EFC cathode at the beginning of each experiment. The first experiment used low enzyme concentration, low initial liquid volume conditions, oxygen for the cathode, and 105% RH. (It should be noted here that the percentages of RH reported herein

[1] Certain trade names and company products are mentioned in the text or identified in an illustration in order to adequately specify the experimental procedure and equipment used. In no case does such identification imply recommendation or endorsement by Georgia Tech., ORNL, or NIST, nor does it imply that the products are necessarily the best available for this purpose.

Table 1
Experimental conditions for imaging experiments at NIST.

Experiment	Enzyme loading (units cm^{-2})	Initial volume (μL)	Feed flow (sccm)	Cathode feed	Cathode humidity (% RH)	Power density ($W m^{-2}$)
1	1	50	50	O_2	105	0.128
2	10	100	10	Air	190	3.49
3	10	100	10	Air	247	4.01

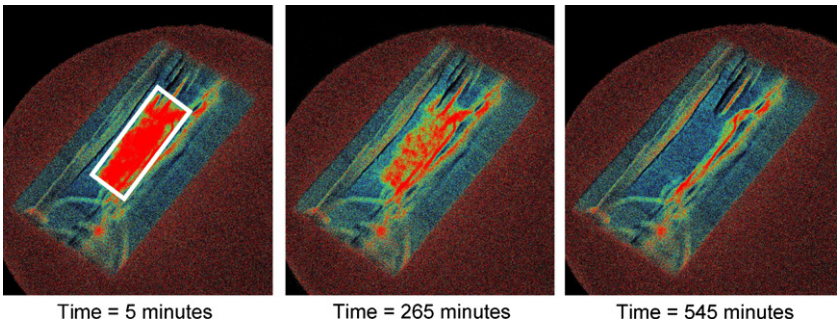

Fig. 2. Neutron images of the operating EFC. The red in the region of interest in the first image (5 min) indicates the presence of water; this region thinned out and disappeared entirely by the end of the experiment (545 min). It can also be seen that the Nafion membrane did not dry out over time (evidenced by the wavy red line).

are with respect to the room temperature.) The second experiment had greater enzyme concentration, a greater initial liquid volume, and supersaturated air (190% RH) at a lower flow rate. The third experiment had conditions similar to the second, but the air was at 247% RH and the enzyme solution had a greater concentration of citrate buffer.

3. Results

Water loss was observed in all the experiments performed at NIST and at ORNL. Fig. 2 illustrates the water loss in a colorized format. These images are from the first experiment: 1 unit of enzyme loading ($U cm^{-2}$), 50 μL initial volume, 50 standard $cm^3 min^{-1}$ (sccm) oxygen flow rate, and 105% RH for the O_2 stream. The white box illustrates the "region of interest" used to calculate cathode water content. It can be seen that water was lost from the cathode of the EFC over time. It is apparent that the PEM maintained a high water content, despite drying of the cathode. In addition, a slow uptake of water by the graphite current collector is also evident. A dry image was taken for 30 min (to provide a well-developed image) prior to injecting solution for each experiment; this image was divided from all "wet" images to yield a change in water content. For all water content results below, the water content was calculated only for the carbon felt region of the cathode (white box in Fig. 2). Water content in the PEM, anode, and current collectors was excluded. In all plots of water content over time measured by neutron radiography, the one-sigma relative uncertainty due to counting statistics was less than or equal to 0.34 μL; thus, uncertainties are not readily visible in the plots.

Fig. 3 shows the cathode water content over 9 h of imaging for experiment 1, with 1 $U cm^{-2}$ and 50 μL initial enzyme solution volume. The maximum power output during this time was 0.128 $W m^{-2}$. A linear fit of the water content profile indicates a water loss rate of 0.051 μL min^{-1}. Fig. 4 shows a similar water content profile for experiment 2, which used 10 $U cm^{-2}$ enzyme loading, 100 μL initial enzyme solution volume, 10 sccm air, and 190% RH. Linear fits of the two series of images taken during this 6-h period indicate a water loss rate of 0.010 μL min^{-1}, representing a fivefold decrease compared with experiment 1. This water loss rate was consistent for the two series of images taken, the second a repeat of the first. The maximum power output during experiment 2 was 3.49 $W m^{-2}$, 27 times greater than that of experiment 1.

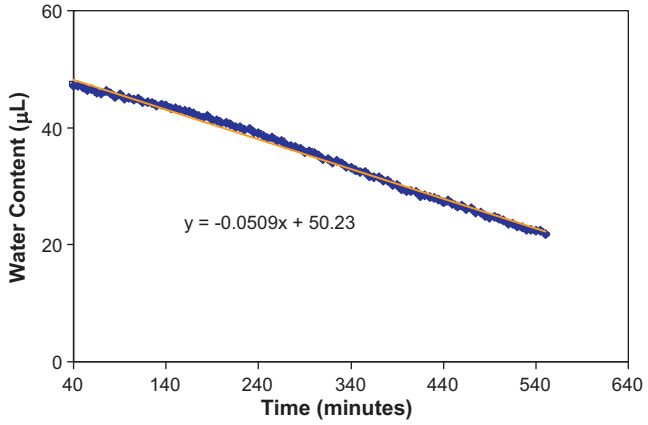

Fig. 3. Time profile of the water content in the EFC cathode. The power output was 0.128 $W m^{-2}$; 50 μL enzyme solution initial; 1 $U cm^{-2}$ enzyme concentration; 50 sccm oxygen; 105 % RH for both feeds. Uncertainty values of 0.32 μL are reported (but not visible) for each data point.

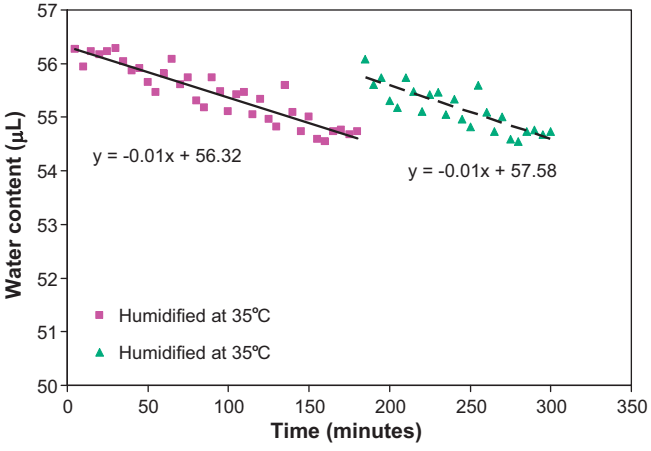

Fig. 4. Water content over time for a supersaturated air condition (190 % RH). Enzyme loading was 10 $U cm^{-2}$; flow rates were 10 sccm for both H_2 and air. The second line represents a duplicate run performed after 3 h of operation.

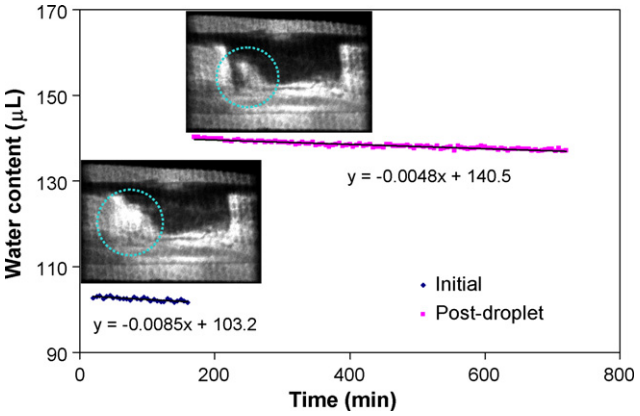

Fig. 5. Water content profile over time for experiment 3 with supersaturated air humidity (247 % RH), 10 U cm^{-2} enzyme loading, 100 μL enzyme solution volume, and increased salt concentration. Inset images show a water droplet that condensed in the cathode input line and was entrained in the cathode. This event, which happened only once, was revealed by neutron radiographs taken before (160 min, bottom picture) and after (165 min, top picture) it occurred.

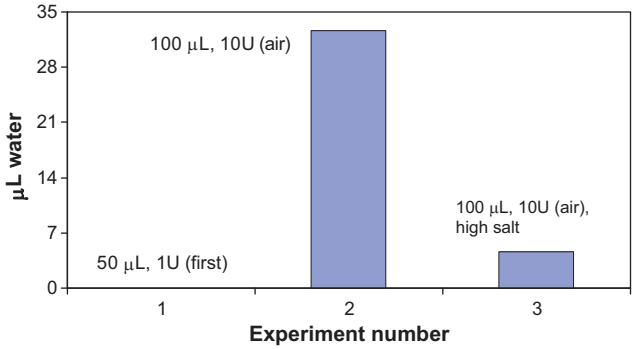

Fig. 6. Comparison of dry images showing that complete drying was not achieved for either experiment following experiment 1. This explains why the initial water volumes for experiments 2 and 3 were not at the expected values (100 μL).

Fig. 5 shows the water content for the final experiment with 10 U cm^{-2} enzyme loading, 100 μL initial enzyme solution volume, 10 sccm air, and 247% RH. In addition, this experiment used a high salt enzyme solution. Over the 8 h of imaging in this experiment, the water loss rate was calculated at 0.005 μL min^{-1}, half that of experiment 2 and one-tenth that of experiment 1. A water droplet entered the cathode just prior to the 200 min mark; this droplet is why the original water volume appears to be near 140 μL. Before- and after-droplet images of the EFC are shown as insets in Fig. 5. While the entire region of water in the cathode is darker, the blue circles also indicate a region that was wetted by the droplet formation (this region had been relatively dry prior to the droplet condensation). It should be noted here that, even with a high relative humidity, only once did a water droplet condense in the air line and enter the cathode of the fuel cell. The result was a sudden jump in the water content, which was captured by neutron imaging as shown in Fig. 5. The maximum power density achieved by the EFC during this experiment was 4.01 W m^{-2}, 15% greater than in experiment 2 and 31 times greater than in experiment 1.

4. Discussion

The reduction in water loss rate observed for experiment 2 compared with experiment 1 likely resulted from nearly all operating conditions being optimized for better output and water retention. The air humidity was much higher, the current and power were much greater (resulting in more product water), and the air flow rate was lower. Switching from O_2 to air and reducing the flow rate were not expected to have had any adverse effect on the power output, as these parameters were above the minimum values established by Borole et al. [2]. The reduction in water loss from experiment 2 to experiment 3 is attributed to increased humidity as well as increased salt concentration in the cathode solution. Such an increase in solute concentration would lower the vapor pressure of the cathode solution, inhibiting evaporation.

It is apparent that the initial water content for both runs in Fig. 4 was approximately 56 μL, rather than the injected 100 μL. This discrepancy is primarily due to the dry image taken as a basis for the series of images used for Fig. 4. The EFC still contained approximately 33 μL of residual water for the dry image used in this series, as seen in Fig. 6. Fig. 6 shows that the "dry" images taken for experiments 2 and 3 reveal some residual water in the cathode; thus, normalizing by the "dry" images from the operating images did not result in true water content. The missing 11 μL of water that should have been measured in experiment 2 is likely due to a droplet of enzyme solution not being in the region of interest used to calculate water content. The region of interest was not changed, however, because inclusion of the membrane and/or cathode current collector would occur.

Mechanisms that affect the water evaporation rate include relative humidity and flow rate of the cathode stream. The effects of relative humidity and cathode flow rate were observed in this work. As expected, increasing the humidity of the cathode stream greatly reduced (by a factor of 10) the water loss rate. However, it is still troubling that water loss was observed for an air stream that was believed to be supersaturated with water as high as 247% RH with respect to room temperature. Thus, further experiments should be performed to explore in greater detail the relationship between water loss rate, air humidity, and flow rate. Increased salt buffer concentration was also observed to have potentially contributed to a reduced water loss rate (by a factor of 2). The salt, in addition to buffering the cathode solution at pH 4, likely contributed to retaining water in the cathode by reducing the vapor pressure of the cathode solution. It is possible that the 5 °C increased temperature of the gas feed lines contributed to the gas not being saturated while fed into the cathode compartment. Despite the EFC being at room temperature, if not enough cooling of the gas occurred upon entering the cathode, it is possible that evaporation could occur from the cathode water layer into unsaturated air. However, cathode drying was also observed in lines that were not heated above the temperature of the saturation bottles, which implies water loss into a saturated air stream [2,5].

Another phenomenon that has been hypothesized to contribute to water loss in the presence of water-saturated air is the increased local temperature as a result of the proton-oxygen-electron water formation reaction that releases heat [15]. Many PEMFC models consider the splitting of hydrogen in the anode to be isothermic while the cathode reaction (production of water from protons, electrons, and oxygen) is exothermic, resulting in a net exothermic reaction [16]. However, electrothermodynamic modeling of a PEMFC performed by Rasmousse et al. [17] suggests the anode reaction could be highly exothermic, while the cathode reaction is slightly endothermic. These studies indicate that a comprehensive understanding of PEMFC heat sources and sinks is still under debate. However, it can be concluded that, due to electrochemical reactions, overall heat production occurs in a PEMFC system. Since the EFC is analogous to the PEMFC design, such an explanation could prove true here, as well. It should be noted that the above thermodynamic modeling studies focused on platinum-based catalysis in a PEMFC; similar studies involving enzyme-based catalysis in an EFC can provide insight on the magnitude of heating or cooling that occurs in an EFC cathode.

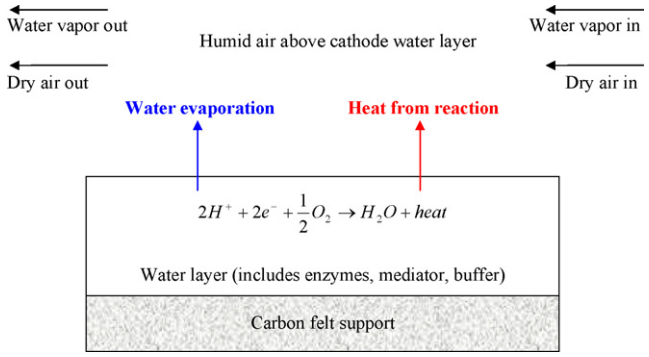

Fig. 7. Schematic of cathode region for mass and heat balances. Steady state is assumed.

Assuming an overall exothermic reaction system, we performed calculations to determine the local temperature in the EFC cathode that would cause the loss of water from the cathode via evaporation. This is of interest because elevated local temperature could cause evaporation of water despite a saturated, bulk stream of air, resulting in the observed water loss. Fig. 7 is a schematic illustrating the system that was used as the basis for the mass and energy balances considered here. A mass balance was performed for the cathode, where the mass flow of water exiting the cathode compartment was the sum of water vapor entering the cathode, water production via the cathode reaction, and water evaporating from the cathode liquid. A net loss of water from the cathode was considered since neutron imaging experiments showed water loss from the cathode. This mass balance is described in Eq. (1). Eq. (2) shows how the rate of water production was calculated from the EFC current.

$$H_2O_{out} = H_2O_{in} + H_2O_{lost} \quad (1)$$

$$H_2O_{produced} = \frac{I}{F} \times \frac{1\,\text{mol } H_2O}{2\,\text{mol } e^-} \times \frac{18\,\text{g}}{\text{mol } H_2O} \quad (2)$$

The "H_2O_{lost}" water stream included the water loss observed via neutron imaging (slopes calculated in Figs. 3–5) as well as the water produced via the cathode reaction (described in Eq. (2)). This is because neutron imaging measured the water content of the EFC cathode; this content would decrease via evaporation but increase due to water production. Thus, the apparent evaporation rate observed via neutron imaging was actually the sum of the loss rate and the rate of production of water. In Eq. (2), I is the EFC current measured in amperes (or $C\,s^{-1}$) and F is the Faraday constant ($mol\,e^-\,C^{-1}$). Since the anode stream was saturated as well, we assumed that the amount of water diffused to or from the anode through the Nafion membrane was negligible. This assumption was supported by neutron imaging results, which showed no appreciable change in anode water content. The entering water flow rate was known since the inlet conditions were experimentally controlled. Water production via the cathode reaction was calculated based on the current at maximum power density (i.e., the condition for which imaging was performed). Finally, water lost from the cathode was determined via the slopes calculated in Figs. 3–5. Addition of the feed and cathode water loss streams composed the exit water stream. This stream of water was converted to absolute humidity. Assuming saturated conditions, we determined the exit temperature of the gas stream based on Lowe and Fick [18] including the amount of evaporated water. Table 2 includes results from the mass balance analysis described here. Note that the experiment with T = 24.5 °C was performed with 100 sccm oxygen, whereas the experiments at 35 °C and 40 °C were performed at 10 sccm air.

It is apparent from Table 2 that most of the water flowing through the cathode compartment of the EFC was from the air feed to the cathode, approximately 97%. The amount of product water resulting from the reaction at the cathode was relatively small. The cathode water loss, however, made up approximately 3% of the water leaving the cathode compartment. Increases in temperature of approximately 0.4 °C are enough to support evaporation that increases the water flow rate from the cathode. Specifically, increased temperatures of 0.4 °C, 0.6 °C, and 0.3 °C for experiments at 24.5 °C, 35.0 °C, and 40.0 °C, respectively, could explain the water loss rates observed in the experiments. The void volume of the cathode compartment was approximately 3 mL, thus the corresponding residence time for the 10-sccm experiments was 18 s. Such a low flow rate is not suspected of entraining water droplets and removing water in bulk. Furthermore, images of the cathode do not indicate migration of water towards the cathode outlet.

To test whether the EFC could provide enough heating to result in such an increase in temperature in the cathode, we performed an energy balance on the cathode. The system for this energy balance can also be seen in Fig. 7. The source of heat in this system was assumed to be the exothermic reaction of protons, electrons, and oxygen to make water. A steady state was assumed. This assumption is supported by a constant water loss rate throughout the experiment. The rate of the cathode reaction was approximated by converting the current developed into moles of water produced and then to heat evolved by that reaction (see Eq. (3)). Thus, for this heat balance, it was assumed that dry air and water vapor entering the cathode must be heated (Eq. (4), with appropriate mass flow and heat capacity for dry air or water). The liquid in the cathode was also a heat sink but was not included since a steady state was assumed. Finally, evaporation of water was considered the final heat sink; this rate was the sum of the water loss observed via neutron imaging and the product water. Eqs. (3)–(5) describe the energy balance discussed here. Pertinent parameters for this heat balance estimation include the heat capacity of dry air and water ($1.004\,J\,g^{-1}\,K^{-1}$ and $4.181\,J\,g^{-1}\,K^{-1}$, respectively), enthalpy of vaporization of water ($2257\,J\,g^{-1}$), and enthalpy of formation of water ($285.8\,kJ\,mol^{-1}$). Table 3 shows the results of this energy balance.

$$Q_{evolved} = \frac{I}{F} \times \frac{1\,\text{mol } H_2O}{2\,\text{mol } e^-} \times \Delta H_f^{H_2O} \quad (3)$$

$$Q_{heating} = \dot{m} C_p \Delta T \quad (4)$$

$$Q_{evolved} \geq Q_{vapor} + Q_{air} + Q_{evaporation} \quad (5)$$

$Q_{evolved}$ is the heat produced via the cathode reaction, $Q_{heating}$ is the amount of energy needed to heat the dry air stream or water vapor, and $Q_{evaporation}$ is the heat needed to evaporate water at the rate observed via neutron imaging. The change in temperature (ΔT in Eq. (4)) corresponded to the temperature increase for each exper-

Table 2
Water mass balance analysis for the calculation of the exit temperature.

T (°C)	Feed water ($\mu L\,min^{-1}$)	Product water ($\mu L\,min^{-1}$)	Cathode water loss ($\mu L\,min^{-1}$)	Evaporated water ($\mu L\,min^{-1}$)	Exiting water ($\mu L\,min^{-1}$)	T exit (°C)
24.5[a]	2.26	8.96E-04	0.051	0.052	2.31	24.9
35[b]	0.398	3.16E-03	0.010	0.013	0.408	35.5
40[b]	0.525	3.86E-03	0.005	0.009	0.530	40.3

[a] 100 sccm oxygen.
[b] 10 sccm air.

Table 3
Heat balance analysis based on calculated temperature increase from Table 2.

T (°C)	Current (A)	Water produced (mol s^{-1})	Heat released from water production (W)		Heat required[c] (W)
24.5[a]	1.60×10^{-4}	8.29×10^{-10}	2.37×10^{-4}	<	2.74×10^{-3}
35[b]	5.64×10^{-4}	2.92×10^{-9}	8.36×10^{-4}	>	7.75×10^{-4}
40[b]	6.89×10^{-4}	3.57×10^{-9}	1.02×10^{-3}	>	5.00×10^{-4}

[a] 100 sccm O_2.
[b] 10 sccm air.
[c] Based on increase in exit temperature (Table 2).

iment shown in Table 2. Finally, as shown in Eq. (5), the heat evolved via the cathode reaction must be greater than the sum of the heat sinks in order for the temperature increases shown in Table 2 to be feasible.

The column in Table 3 titled "Heat released from water production" refers to the enthalpy of formation of water released at a rate based on the current of the EFC. The column titled "Heat required" refers to the amount of energy input necessary to increase the temperature of the air and water vapor by the temperature increases in Table 2. In addition to heating those components of the cathode, heat to cause evaporation at the rate predicted using the data obtained via neutron imaging observations (Table 2) was considered. It can be seen in Table 3 that it was feasible for a slight increase in temperature (~0.4 °C) to occur based on the heat released by the reaction that occurred in the cathode. This is indicated by observing that the energy released via the cathode reaction is in excess of the heat required to increase the temperature by the amounts shown in Table 2 (for experiments 2 and 3). It is noted that other heat sources and sinks were likely to exist in the operating EFC. These results, however, indicate that enough heat can be evolved in the cathode to support slightly increased temperature throughout the liquid and gas phases of the cathode. It is possible that, in an EFC optimized for increased power production, water loss due to evaporation as described above can be more pronounced than in the work presented here.

It is also possible that the cathode water loss was influenced by the heated feed lines in the experiments performed at NIST. These lines were maintained at a temperature 5 °C above the temperature of the humidification bottles. Since the temperature increase calculated in the cathode was only an average of 0.4 °C for the three experiments, it could be possible that heating the lines caused the air to be unsaturated, allowing evaporation to occur. However, it is evident in Fig. 5 that the feed inlet for the air side resulted in a droplet of water entering the cathode in experiment 3. This suggests that condensation could occur in the line, so the air side was saturated. In addition, experiments performed at ORNL with unheated lines and saturated air also exhibited water loss. Thus, although the heated lines at NIST could be one of the reasons for water evaporation from the cathode, cathodic reactions can still produce enough heat to instigate evaporation even for a saturated inlet air stream.

Additional experiments have been performed in which an EFC with aluminum, rather than PTFE, endplates was used. As visible in Fig. 2, the Nafion PEM was not flat but was wavy as a result of being in contact with the tie rods that held the end plates together. The anode also appears to be at a slight angle to the PEM instead of being parallel to it. The rigid aluminum endplates that were used in the second generation experiments minimized these effects. A new 40 mm cross strip detector with an imaging resolution of 10 μm was also used in the follow-up experiments. Also, these experiments involved an EFC with relatively low current density, although it exhibited a high volumetric power density (1.07 kW m^{-3}). Further work should include EFCs with higher current density and incorporate the three-dimensional, porous, flow-through design of the current EFC. Finally, an effort should be made in future work to accurately measure the temperature in the cathode compartment of the modified EFC to verify the mass balance findings.

5. Conclusion

The water content in the cathode of an operating EFC was successfully measured and studied. Neutron imaging was demonstrated to be a useful technique for exploring the water-loss behavior and for quantifying the rate of water loss; this is important since water balance is an important aspect of EFC operation. The water loss from the cathode can possibly be explained by a local increase in temperature in the cathode; the consequence of such a local increase is that the air stream became unsaturated in the cathode, causing evaporation. Thermodynamic studies would be of great interest to understand the general EFC operation, as well as commonly observed water loss. Separation of water loss and enzyme/mediator degradation contributions to EFC power loss can be achieved by implementing neutron imaging as a tool in EFC studies. A better understanding of such contributions to power loss can lead to improvements in the design and operation of EFCs, increasing available power from these devices.

Acknowledgments

This work was supported by the American Chemical Society, Petroleum Research Fund – Green Chemistry Initiative at Georgia Institute of Technology. EFC work at Oak Ridge National Laboratory was supported by the Laboratory Directed Research and Development Program of ORNL. Oak Ridge National Laboratory is managed by UT-Battelle, LLC, for the U.S. Department of Energy under contract DE-AC05-00OR22725. Neutron imaging was performed at the National Institute of Standards and Technology, Center for Neutron Research. The authors acknowledge Mr. Eli Baltic of the NIST for technical assistance in carrying out the neutron radiography experiments. This work was supported by the U.S. Department of Commerce, the NIST Ionizing Radiation Division, the Director's office of NIST, the NIST Center for Neutron Research, and the Department of Energy through Interagency Agreement No. DE-AI01-01EE50660.

References

[1] P. Atanassov, C. Apblett, S. Banta, S. Brozik, S.C. Barton, M. Cooney, B.Y. Liaw, S. Mukerjee, S.D. Minteer, Electrochem. Soc. Interface 16 (2007) 28–31.
[2] A.P. Borole, S. LaBarge, B.A. Spott, J. Power Sources 188 (2) (2009) 421–426.
[3] J. Liu, M. Esai Selvan, S. Cui, B.J. Edwards, D.J. Keffer, W.V. Steele, J. Phys. Chem. 112 (6) (2008) 1985–1993.
[4] S.D. Minteer, B.Y. Liaw, M.J. Cooney, Curr. Opin. Biotechnol. 18 (2007) 1–7.
[5] N.S. Hudak, J.W. Gallaway, S.C. Barton, J. Electrochem. Soc. 156 (1) (2009) B9–B15.
[6] W. Gellet, J. Schumacher, M. Kesmez, D. Le, S.D. Minteer, J. Electrochem. Soc. 157 (4) (2010) B557–B562.
[7] A. Zebda, L. Renaud, M. Cretin, C. Innocent, R. Ferrigno, S. Tingry, Sens. Actuators B-Chem. 149 (1) (2010) 44–50.
[8] I. Ivanov, T. Vidakovic-Koch, K. Sundmacher, Energies 3 (4) (2010) 803–846.
[9] R. Satija, D.L. Jacobson, M. Arif, S.A. Werner, J. Power Sources 129 (2004) 238–245.
[10] Y.S. Chen, H. Peng, D.S. Hussey, D.L. Jacobson, D.T. Tran, T. Abdel-Baset, M. Biernacki, J. Power Sources 170 (2) (2007) 376–386.

[11] D.S. Hussey, D.L. Jacobson, M. Arif, J.P. Owejan, J.J. Gagliardo, T.A. Trabold, J. Power Sources 172 (1) (2007) 225–228.
[12] M.A. Hickner, N.P. Siegel, K.S. Chen, D.S. Hussey, D.L. Jacobson, M. Arif, J. Electrochem. Soc. 155 (4) (2008) B427–B434.
[13] D.S. Hussey, D.L. Jacobson, M. Arif, K.J. Coakley, D.F. Vecchia, J. Fuel Cell Sci. Technol. 7 (2010) 021024-1.
[14] T.A. Trabold, J.P. Owejan, J.J. Gagliardo, D.L. Jacobson, D.S. Hussey, M. Arif, in: W. Vielstich, H. Yokokawa, H.A. Gasteiger (Eds.), Handbook of Fuel Cells – Fundamentals, Technology and Applications. Volume 6: Advances in Electocatalysis, Materials, Diagnostics and Durability, John Wiley & Sons, Ltd., 2009, ISBN:978-0-470-72311-1.
[15] M.A. Hickner, N.P. Siegel, K.S. Chen, D.N. McBrayer, D.S. Hussey, D.L. Jacobson, M. Arif, J. Electrochem. Soc. 153 (2006) A902.
[16] H. Wu, P. Berg, X. Li, J. Power Sources 165 (2007) 232–243.
[17] J. Rasmousse, O. Lottin, S. Didierjean, D. Maillet, J. Power Sources 192 (2009) 435–441.
[18] P.R. Lowe, J.M. Ficke, The computation of saturation vapor pressure. Tech. Paper No. 4-74, Environmental Prediction Research Facility, Naval Postgraduate School, Monterey, CA, 1974.